nature communications

Article

https://doi.org/10.1038/s41467-025-57121-0

Heterogeneous Earth's mantle drilled at an embryonic ocean

Received: 5 October 2024

Accepted: 11 February 2025

Published online: 27 February 2025

Check for updates

Alessio Sanfilippo[1] ✉, Ashutosh Pandey[2], Norikatsu Akizawa[3], Eirini Poulaki[4], Emily Cunningham[5], Manon Bickert[6], Chao Lei[7], Paola Vannucchi[8], Emily R. Estes[9], Alberto Malinverno[10], Noriaki Abe[11], Agata Di Stefano[12], Irina Y. Filina[13], Qi Fu[14], Swanne B. L. Gontharet[15], Lorna E. Kearns[16], Ravi Kiran Koorapati[17], Maria Filomena Loreto[18], Luca Magri[19], Walter Menapace[20], Victoria L. Pavlovics[5], Philippe A. Pezard[21], Milena A. Rodriguez-Pilco[22], Brandon D. Shuck[4], Xiangyu Zhao[23], Carlos Garrido[24], Daniele Brunelli[25], Tomoaki Morishita[26] & Nevio Zitellini[18]

Mantle processes control plate tectonics and exert an influence on biogeochemical cycles. However, the proportion of mantle sampled in-situ is minimal, as it is buried beneath igneous crust and sediments. Here we report the lithological characteristics of two mantle sections from an embryonic ocean drilled by the International Ocean Discovery Program (IODP) in the Tyrrhenian Sea. Contrary to the mantle drilled at Mid Ocean Ridges (MORs) and hyper-extended passive margins, our findings reveal exceptionally heterogeneous and fertile mantle lithologies, ranging from fertile lherzolites to depleted harzburgites and dunites, interlayered with pyroxenites. Plagioclase- and clinopyroxene-rich layers, hydrous potassic magmatic veins, and mafic intrusions indicate substantial mantle refertilization and delayed inception of magmatic crust. We propose that magma-poor rifts do not require a chemically depleted mantle, too refractory to melt. Deep lithospheric processes such as mantle refertilization and prolonged lithospheric thinning delayed melt focusing and the formation of a steady-state spreading center.

Since the discovery of large portions of the upper mantle exhumed at slow and ultraslow spreading MORs, scientific ocean exploration programs have aspired to collect in-situ sections of the underlying mantle (Fig. 1a and Table 1). Currently, drilled sections of the oceanic mantle are limited to three locations along the central Mid-Atlantic Ridge - near the Kane Fracture Zone at 23°N (Ocean Drilling Program, ODP Leg 153)[1], at the 15°20' N Fracture Zone (ODP Leg 209)[2], and recently in the Atlantic Massif oceanic core complex at 30°N (IODP Expedition 399)[3]. The mid-oceanic mantle section in the Pacific Ocean has only been drilled in the Hess Deep[4], a tectonic window along the East Pacific Rise, during ODP Leg 147. The abyssal mantle peridotites recovered at these sites are extensively serpentinized and geochemically depleted due to partial melting of the ascending asthenosphere. Clinopyroxene-poor peridotites, such as harzburgites and dunites, are the most commonly drilled mantle lithologies at these sites and rarely consist of plagioclase-rich varieties, formed in response to grain-scale percolation and crystallization of MOR basaltic (MORB) magmas[5]. In addition, a significant proportion of these depleted mantle sections consist of MORB-type magmatic intrusions of variable thickness (Table 1).

In addition to MORs, mantle peridotites in the ocean have also been recovered in the distal portion of a passive continental margin, a geological setting that formed during the last phase of continent rifting, which is well distinct from that of a mature ocean ridge. In the late 20th century, the discovery of these exhumed mantle rocks by drilling during ODP Legs 103, 149, 173, and 210 at the conjugate magma-poor Iberia-Newfoundland rifted margins in the Atlantic Ocean[6,7], led to the

A full list of affiliations appears at the end of the paper. ✉e-mail: alessio.sanfilippo@unipv.it

https://doi.org/10.1038/s41467-025-57121-0

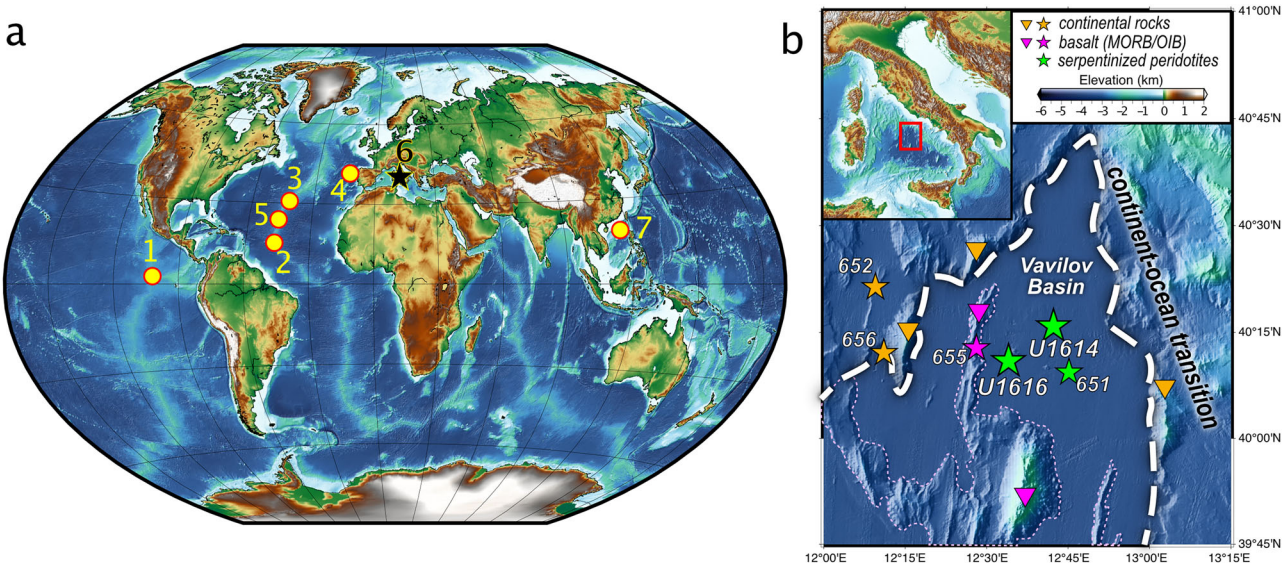

Fig. 1 | Locations of DSDP-ODP-IODP drilling sites recovering > 50 m thick mantle peridotite sections. a 1 – ODP Leg 147 (Hess Deep, East Pacific Rise), 2 – ODP Leg 153 (Kane Fracture Zone, Mid-Atlantic Ridge), 3 – ODP Leg 209 (15°20' Fracture Zone, Mid-Atlantic Ridge), 4 – ODP Leg 173 (Western Iberian margin COT, Atlantic Ocean), 5 – IODP Expedition 399 (Atlantis Massif, Mid-Atlantic Ridge). 6 – IODP Expedition 402 (Tyrrhenian Sea), this study. The location of IODP Expeditions 367-368 in the South China Sea COT is also shown (7). **b** Bathymetrical map and location of the Expedition 402 sites (U1614 and U1616) in the Vavilov basin (Tyrrhenian Sea). Previous drill sites and results of dredging are also shown (Sites 651, 652, 655, and 656). Colors refer to the nature of the recovered basement lithologies. White lines mark the location of interpreted normal faults.

Table 1 | List of the ocean drilling expeditions in which > 50 m mantle peridotite sections have been sampled

Expedition	Holes and total recovery	Location	Recovered mantle rocks and associated mafic lihologies
ODP Leg 147	Holes 895 A, 895B, 895 C, 895D, 895E, and 895 F (recoveries:13.8%, 9.9%, 15.1%, 21.4%, 37.1%, and 7.6%)	Hess Deep (East Pacific Rise)	Harzburgite (44%) and dunite (43%), with mafic lithologies (13%) comprising troctolite, gabbro, and rare diabase
ODP Leg 153	Holes 920B and 920D (recoveries: 39.7% and 47%)	Kane Fracture Zone (Mid-Atlantic Ridge)	Almost entirely constituted of harzburgite and minor dunite, with rare gabbro and diabase
ODP Leg 173	Holes 1068 A and 1070 A (recoveries: 43.2%, 73.9%)	Western Iberian margin ocean-continent transition (Atlantic Ocean)	Harzburgite and minor lherzolite and plagioclase-bearing lherzolite, with minor gabbro
ODP Leg 209	Holes 1268 A, 1270 A, 1270B, 1270 C, 1270D, 1271B, 1272 A, 1274 A, and 1275 A (recoveries: 53.3%, 12.2%, 37.4%, 10.6%, 13.4%, 15.3%, 28.6%, 22.2%, and 2.6%)	15°20′ Fracture Zone (Mid-Atlantic Ridge)	Harzburgite and dunite, with troctolites and gabbro
IODP Expedition 399	Holes U1601A and U1601C (recoveries: 24% and 71%)	Atlantis Massif (Mid-Atlantic Ridge)	Harzburgite (82%), dunite (18%) with gabbro and rare diabase and basalt
IODP Expedition 402	Holes U1614C and U1616E (recoveries: 45% and 21%)	Tyrrhenian ocean-continent transiton, Mediterranean Sea	Lherzolites (43% in Hole U1614C and 28% in Hole U1616E), harzburgite (32% in Hole U1614C and 57% in Hole U1616E) and dunites (including plagioclase-bearing varieties) (11% in Hokle U1614C and 3% in Hole U1616E), pyroxenites (4% in Hole U1614C and 1% in Hole U1616E) with rare gabbro and hydrous mafic magmatic veins (3% in Hole U1614C and 9% in Hole U1616E)

The proportion of mantle rocks is mentioned next to the lithology wherever available. See text for details.

formulation of a new model for the formation of Continent – Ocean Transition (COT). Prior to this, the COT was interpreted as a simple juxtaposition of stretched continental crust and new magmatic oceanic crust resulting from rapid lithospheric breakup and leading to a magmatically robust mid-ocean ridge system. Drilling offshore at the hyper-extended Atlantic-COT challenged this axiom, showing that continental breakup can be followed by exhumation of a chemically depleted sub-continental mantle with minimal or absent magma production, until the uprising asthenosphere produced enough melts and focused melt-extraction to generate a magmatic Penrose-type oceanic crust[6,8]. Over the past decades, COT has been thereby classified into two end-member models of magma-rich and magma-poor types, characterized by contrasting structural architectures[9,10]. Despite a global consensus that the magma-poor nature of hyper-extended COTs is caused by a combination of low extension rates and a depleted nature of the lower lithospheric mantle[11–17], the debate is still ongoing due to a lack of direct geologic sampling to test geophysical observations and geodynamic models of these contrasting end-members. The IODP Expeditions 367-368 drilled the intermediate South China Sea (SCS) continental margin and recovered unexpectedly thick MORB-type basaltic sections close to the thinned continental crust, revealing that abundant magmatism was produced during the breakup

of a thinned continental lithosphere[18]. The mechanical behavior of the lithosphere, which is also dependent on its inherited structures, exerts a key influence on the rifting evolution[19]. Hence, understanding the COT formation requires access to deep lower crustal and mantle rocks to define the link between deep tectono-magmatic processes and the development of a rifted margin.

Exhumed mantle in the central Tyrrhenian Sea embryonic ocean

Continuing the legacy of in-situ mantle drilling in COT, the penultimate IODP Expedition (402) on the R/V JOIDES Resolution was conducted to drill into the oceanic basement of the Vavilov Basin, representing an embryonic oceanic basin located in the central part of the Tyrrhenian Sea (Fig. 1b). Different from the Iberia-Newfoundland rifted margins, the COT exposed in the area never developed a steady-state ocean ridge, and shares geological features with both magmatic and amagmatic COTs. The Tyrrhenian Sea was formed as a result of the northwestward subduction of the Ionian oceanic lithosphere beneath the Calabrian Arc and slab roll-back[20–23]. This process stretched a thinned continental lithosphere, which may have included remnants of the Jurassic Alpine Tethys, to create an active back-arc basin. Lithospheric thinning began in the southern part of the Tyrrhenian during the Middle Miocene. With the rate of extension increasing progressively, lithospheric thinning moved southward until it breaks at latitude 41°N, leading to the opening of the Vavilov basin[23] (Fig. 1b). Seismic data[22,23] and previous drilling expeditions[24] concur that the central portion of the Vavilov basin is formed by exhumed mantle peridotites covered by a thin layer of basalts and sediments. Although the basin opened at a full spreading rate ranging between 40 and 60 mm/yr[21], which is higher than ultraslow and slow-spreading ridges where mantle exhumation has been largely reported, the absence of a continuous magmatic crust suggests regional igneous starvation. The main objectives of IODP Expedition 402 were to ascertain whether the mantle in this nascent ocean differs from the depleted mantle observed at MORs and at Atlantic-type hyper-extended COTs and to constrain the effect of mantle composition in the transition from continental rifting to ocean formation.

Results

The post-Messinian (< 5 Ma) basement of the Vavilov basin was the focus of scientific drilling during the 1980s and 1990s when DSDP Site 373 and ODP Site 655 recovered exclusively < 150 m thick MORB-type tholeiitic basalts along linear ridges trending N10°E[24]. Only ODP Site 651 (Leg 107) recovered a 40 m thick mantle section, below 136 m of basalts and basalt breccias, intercalated by a dolerite-albitic intrusion[25]. The drilled peridotites were extensively serpentinized, and the original mantle fabric showed porphyroclastic textures with relicts of orthopyroxene and spinel in a serpentinized matrix. In contrast, IODP Expedition 402 recovered two continuous sections of moderately to highly serpentinized mantle peridotites (Sites U1614 and U1616) directly beneath a ~ 250 m thick sedimentary cover, with no intervening magmatic crust (Fig. 2). The contact between brecciated serpentinized peridotites and dolomitic sediments is exceptionally preserved (Fig. 3a) and lack a thick zone of cataclasites or tectonic gouges as observed at the top of exhumed mantle in other COT[6,7]. Ophicarbonates and tectonic breccias were nonetheless recovered at different stratigraphic levels throughout both Expedition 402 sites (Supplementary Figs. 1, 2). The 160 m thick mantle section sampled at Site U1614 is composed of approximately equal proportions of spinel-bearing lherzolite (24%) and harzburgite (26%), with minor dunite (10%), pyroxenites (4%) and mafic intrusions (3%) (Fig. 2a and Supplementary Fig. 1). Plagioclase-bearing lherzolites and harzburgites constitute the rest of the mantle section (27%). The 94 m thick mantle section cored at Site U1616 also recovered heterogeneous lithologies with spinel-bearing harzburgites and lherzolites making up to 50% and 19% of the recovered fraction, respectively (Fig. 2b and Supplementary Fig. 2). Mafic intrusions in both U1614 and U1616 mantle sections are relatively abundant and dispersed throughout the section (Figs. 2c, 3b–d). The different lithologies appear randomly distributed throughout the two sites. However, depleted harzburgites and dunites are prevalent at shallower depths at Site U1614 (< 320 mbsf). The results of Expedition 402 are in good agreement with the refractory nature of the peridotites previously sampled at ODP Site 651[26], which were restricted to a depth of 30 m below the sedimentary cover. The thicker mantle sections drilled at Sites U1614 and U1616 now suggests that refractory peridotites (26% at Site U1614 and 50% at Site U1616) are not prevailing lithologies in the Tyrrhenian COT mantle, which is exceptionally heterogeneous and on average mineralogically fertile. The relative proportions of fertile lithologies in the Tyrrhenian mantle are indeed exceptionally higher than mantle peridotites available from back-arc and fore-arc oceanic basins, with a lithological heterogeneity covering the entire spectrum of MOR mantle peridotites (Fig. 4). Notably, the clinopyroxene modal proportions of Hole U1416C peridotites exceed by far that of Hole U1601C that drilled a 1268 m long section of depleted mantle at the Mid-Atlantic Ridge[5].

Discussion

Mantle heterogeneity, deformation and melt refertilization

The recovered dunites likely formed as a response to focused melt migration[27,28]. This inference is based on the occurrence of large quantities of chrome-spinel organized in subparallel trails, defining a foliation that is geometrically consistent with the harzburgite contacts and mantle fabric dips (Supplementary Figs. 1, 2). In addition, some of the dunites contain plagioclase and diopside-rich veins, reflecting the reactive percolation of melts at lower temperatures[29,30]. Consistently, the TiO_2 contents of the dunite locally reached 0.05 wt %, lower than those of the harzburgites (typically 0.01-0.02 wt%) suggesting chemical equilibration with migrating melts (Fig. 5a). Conversely, the sampled harzburgites rarely contain plagioclase, instead preserving a refractory chemical character (Supplementary Figs. 1, 2). These harzburgites are compositionally more depleted than most of the abyssal peridotites sampled from MORs and the Iberia-Newfoundland COT, approaching the composition of fore-arc peridotites from the Mariana Trench that have undergone hydrous-fluid flux melting forming arc-related magmas (Fig. 5). Although some of the depleted Tyrrhenian harzburgites seem to be similar to fore-arc peridotites, a suprasubduction tectonic setting would not explain the geochemical signature of the basalts recovered in the Vavilov Basin and Vavilov Seamount that range from MORB-like to alkaline[24,26]. The very low Al_2O_3, TiO_2, K_2O, and CaO contents of the Tyrrhenian harzburgites (Fig. 5 and Supplementary Fig. 3), instead, can be explained by high degree (~ 20–25%) fractional melting of a typical depleted mantle peridotite (Fig. 5; see detail of the melting model in figure caption and in Supplementary Data 4). Such a residual character is also revealed by the low incompatible trace element compositions (i.e., mid to heavy-Rare Earth Elements) of pyroxene from the Site 651 peridotites, indicating high degrees of partial melting and melt extraction. The paucity of magmatic features, such as volcanic ridges and seamounts, indicates a subdued melt supply in the Tyrrhenian Sea[22], the refractory character could have been partly inherited from ancient melting events. Ancient refractory mantle domains are documented in mantle sections from the Jurassic Alpine ophiolites[31] and the subcontinental lithospheric mantle (SCLM) exposed in the Ivrea-Verbano Zone of the Southern Alps[32], proving that refractory portions of mantle are entrained in the circum-Tyrrhenian SCLM[33]. Therefore, although we cannot exclude that some of the collected peridotites melted to some degrees during the rifting stage, the existence of highly depleted harzburgites in the Tyrrhenian mantle may be related to ancient melting events that preceded continental rifting and opening of the basin, as seen in the surrounding subcontinental peridotites.

https://doi.org/10.1038/s41467-025-57121-0

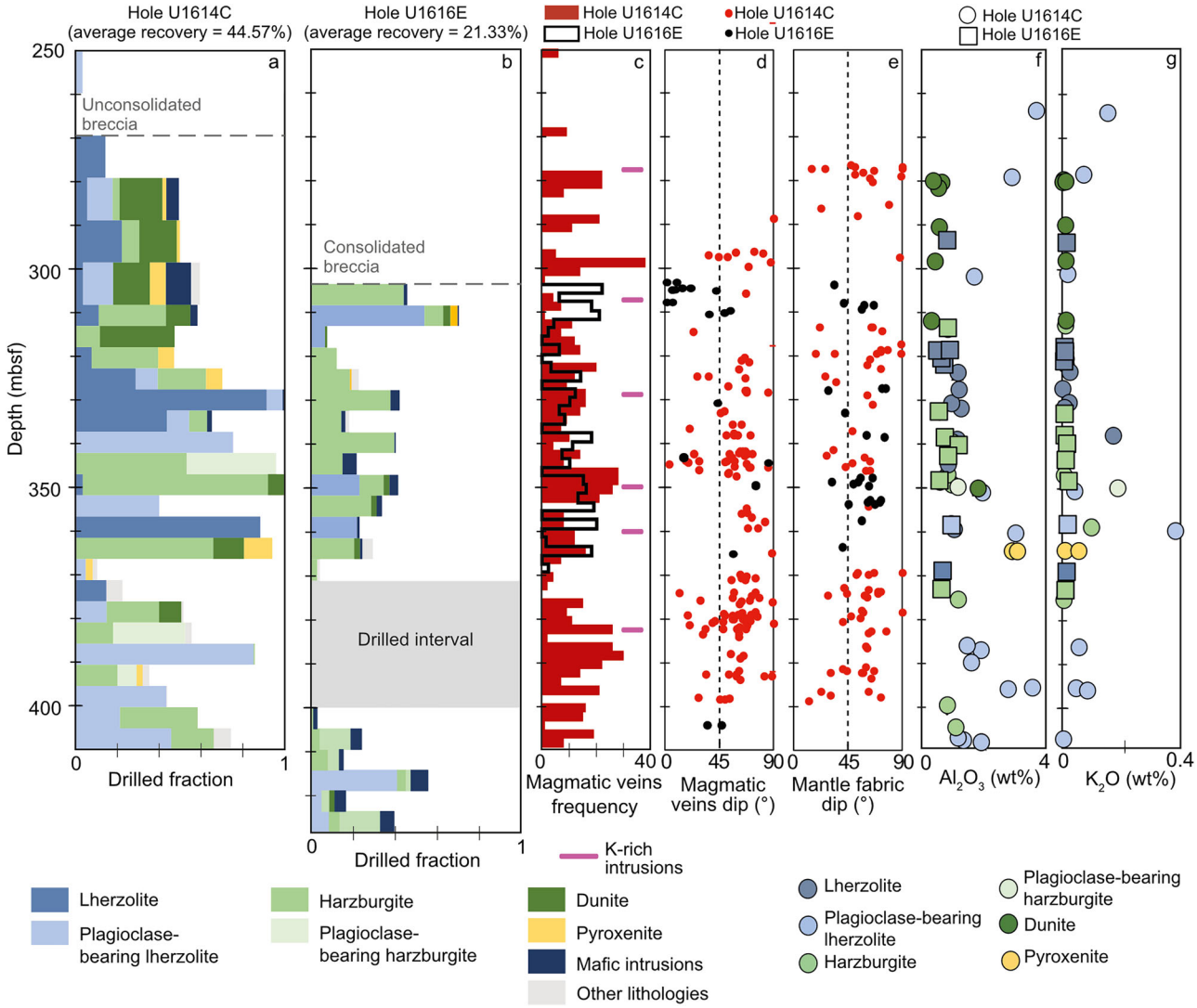

Fig. 2 | Stratigraphy of the drilled holes where mantle sections are recovered during IODP Expedition 402. a and (**b**) show lithostratigraphy of Holes U1614C and U1616E, respectively. **c** Depth-wise variation in magmatic vein intensity calculated at 2 m intervals for both holes. Magmatic veins group all veins with primary minerals including pyroxene-rich, plagioclase-rich, and gabbroic intrusions. Dip of magmatic veins (**d**) and mantle ductile fabric (**e**) relative to the core reference frame. Also indicated are the locations of K-Ti-rich mafic intrusions (pink bars). Depth-wise whole rock (**f**) Al_2O_3, and (**g**) K_2O variations in peridotites. The gray bar in Hole U1616E indicates a drilled interval with no coring.

These depleted harzburgites are widespread in the Tyrrhenian COT mantle, where they are associated with significant quantities of mineralogically and chemically fertile peridotites (lherzolites) and pyroxenites. The lherzolites have a porphyroclastic texture with weak foliation defined by the preferential orientation of pyroxene and spinel (Fig. 3b). This coarse-grained, high-temperature protogranular texture is characteristic of asthenospheric flow[34]. This fabric locally evolves to highly deformed horizons with strong oriented crystal-plastic fabrics and mylonitic textures, likely related to exhumation and formation of low-angle normal faults (Supplementary Figs. 1 and 2). Most of the lherzolite layers show weak plastic deformation and have undeformed plagioclase organized in millimeter-scale trails, often aligned along the main foliation of the pyroxene porphyroclasts and spinels (Fig. 3b), attesting to melt impregnation following the deformation process. The lherzolites extend from refractory compositions to a very fertile character, represented by plagioclase-bearing lherzolites, which preserve covariations in Al_2O_3 versus MgO, CaO, TiO_2, and K_2O contents (Fig. 5a, b and Supplementary Fig. 3). Plagioclase crystallizes in response to refertilization or impregnation by migrating melts at lithospheric levels[35], and is a well-known process at slow-spreading MORs[36], COTs[13], and back-arc basins[35]. However, the Tyrrhenian mantle also shows textural evidence for crystallization of secondary clinopyroxene in veins ranging in thickness from mm- to cm (Figs. 3b, 6), which are instead rare in the sub-ridge mantle[37]. Clinopyroxene can crystallize from mafic melts at high pressure or due to the interaction of alkaline melts with the host peridotites[36,38,39], conditions that can convert initially depleted harzburgites into fertile lherzolites. Given that alkaline melts are widespread from the Vavilov and Magnaghi seamounts (Fig. 1b), both located in close vicinity to the drilled sites[40], similar melts might have migrated and interacted with the peridotites since the early phases of exhumation of the mantle sequence. Evidence for early interaction with alkaline melts is indeed documented in ODP Site 651 peridotites, where interstitial clinopyroxene presenting selective enrichments in strongly incompatible elements is locally associated with magmatic amphibole, preserving evidence of high-temperature deformation related to mantle exhumation[41]. Refertilization by interaction with alkaline melts is also consistent with the slight but distinct K_2O enrichment observed in many plagioclase-bearing

https://doi.org/10.1038/s41467-025-57121-0

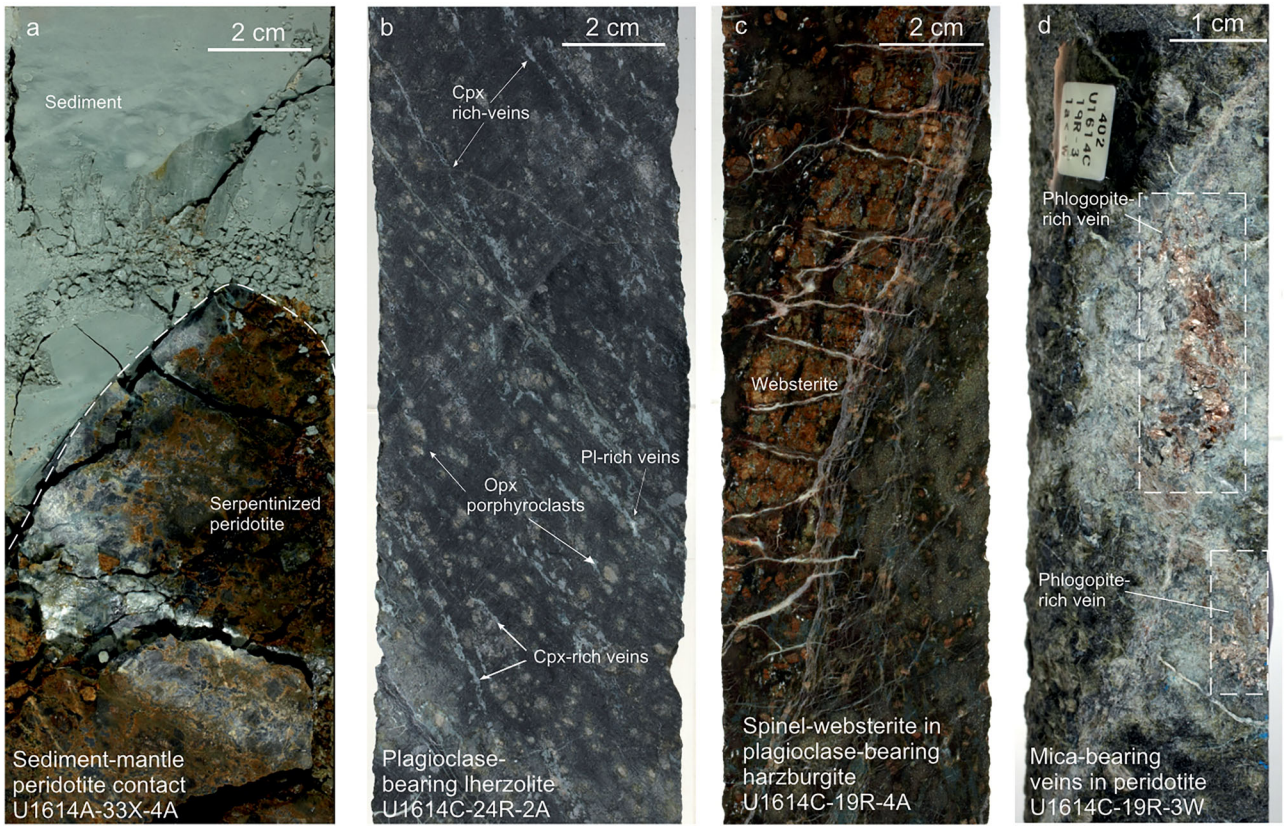

Fig. 3 | Representative core section images of IODP Site U1614 peridotites. a The sediment-basement interface is defined by a direct contact (white dashed line). Peridotite is highly serpentinized with a weak mantle fabric defined by the alignment of pyroxene minerals. **b** Clinopyroxene and plagioclase-rich veins in partially serpentinized peridotite at a low angle to the mantle fabric orientation defined by orthopyroxene porphyroclasts. **c** Weathered plagioclase-bearing harzburgite intruded by a centimeter-scale spinel-websterite vein. The latter is rimmed by serpentine and carbonate veins and fractured by another, orthogonal network of the same veins. **d** Phlogopite-rich veins hosted in mantle peridotite.

peridotites (Fig. 5b, d) and is rarely seen in global MOR peridotites. The K_2O enrichments are nonetheless also found in mantle peridotites from the Iberian COT and the Philippine Sea back-arc basin (Fig. 5d), suggesting the occurrence of alkaline melts during the refertilization process of the transitional mantle. Hence, although defining the timing of depletion and refertilization requires further investigations, the geometric relationships between deformation and melt-migration features and the geochemical affinity of refertilizing melt leads us to propose that the plagioclase and clinopyroxene-rich veins within the lherzolites were generated by localized events of refertilization during the exhumation of the mantle sequence to the Tyrrhenian seafloor. We cannot exclude, however, that some of the chemical variability observed here could have been acquired during ancient events of refertilization, similar to what has been suggested for fertile SCLM sections exposed in the circum-Mediterranean area[42] (Fig. 5). In any case, ancient and recent refertilization processes resulted in a high chemical variability of this embryonic oceanic mantle sequence that encompasses the full range of chemical variability of abyssal peridotites from oceanic tectonic settings in only two drill sites (Figs. 4, 5 and Supplementary Fig. 4).

Concrete evidence supporting the heterogeneous character of the Tyrrhenian mantle is the presence of a minor (~ 4%) yet significant proportion of pyroxene-rich lithologies, such as websterites, orthopyroxenites, and clinopyroxenites. These fertile and readily fusible lithologies, grouped as 'pyroxenites', are recovered throughout both mantle sections, where they have thicknesses ranging from 3 cm to as high as 10 cm (Fig. 3c). The best-preserved pyroxenite occurrences are the subparallel layers of spinel websterites in plagioclase-bearing harzburgites recovered at ~ 230 mbsf at Site U1614 (Fig. 3c and Supplementary Fig. 1). Unlike the spinel trails in plagioclase-peridotites, the coarse pyroxene porphyroclasts composing the pyroxenites veins are weakly deformed, showing undulose extinction, which is consistent with the overall weak deformation of the host peridotite. The websterites contain abundant ameboid-shaped mm-sized Cr-spinels. Plagioclase rims around spinel within pyroxene-rich domains attest to melt impregnation, or sub-solidus re-equilibration from spinel to plagioclase-facies mantle conditions[43]. The subtle enrichments in CaO, Al_2O_3, and TiO_2 at constant Mg# distinguish these chemical fertile mafic lithologies from most of the peridotites (Fig. 5a, b and Supplementary Fig. 3). In orogenic massifs, pyroxenites are common lithologies, and appear stretched, boudinaged, and intermingled with the host SCLM peridotites. These pyroxenites are either considered to be formed as a result of recycling crustal material[44], or from high-pressure segregation of melts with remarkable crustal components[45]. At MORs, pyroxenite layers are rare and commonly interpreted as deep segregations of melt contemporary to the MORB magmatism[46]. None of these hypotheses can be discounted here, but, in all cases, the coexistence of these fertile lithologies with highly refractory peridotites and lherzolites attest that a compositional heterogeneity was attained during events of refertilization processes following the last melting event.

Most of the Tyrrhenian samples have retained a weak, porphyroclastic texture, typical of the high temperature, and low stress conditions expected in the asthenospheric mantle or the deep lithosphere[47]. Peridotites with higher degrees of deformation, such as protomylonites to mylonites, are mostly associated with mafic veins

https://doi.org/10.1038/s41467-025-57121-0

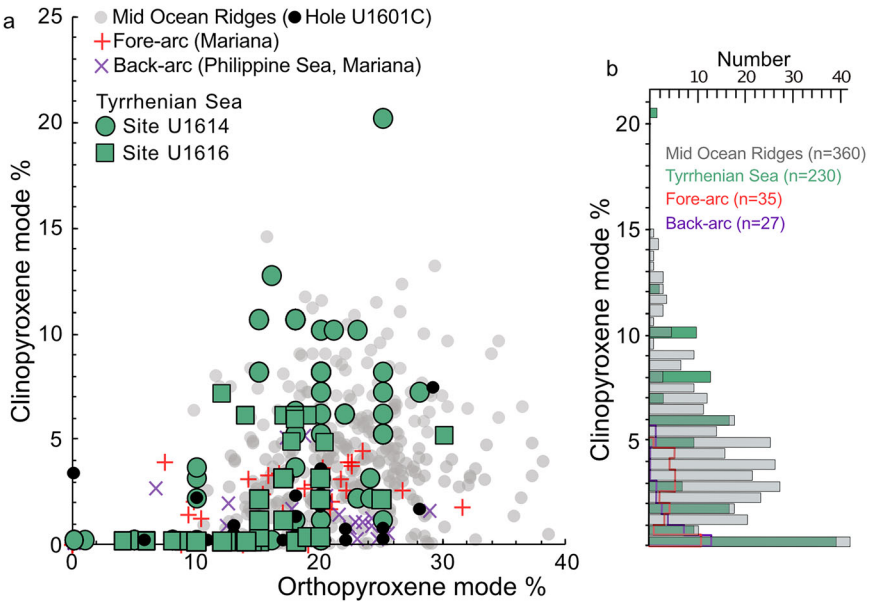

Fig. 4 | Mineral abundance in Sites U1614 and U1616 peridotites. a Relationships between orthopyroxene and clinopyroxene modal abundances and (**b**) histogram of clinopyroxene modal abundance compared to peridotites from mid-ocean ridges[5,37] (gray plain bars), fore-arc[54] (red contours) and back-arc[55,56] (purple contours).

that intrude the exhumed peridotites and rarely reported in the depleted lithologies (Supplementary Figs. 1, 2). In the refertilized peridotites, this high-temperature fabric is sub-parallel to the plagioclase and clinopyroxene-rich trails formed as response to the refertilization process (Figs. 2, 3, 6a, b). The prevalence of this high-temperature low-stress deformation in refertilized lherzolites and of mafic veins is a fundamental observation, as it suggests that detachment faults exhuming these mantle rocks likely root into a domain in which the mantle was weakened by regular melt injections. In addition, similar geological observations attesting for melt-rock interaction and melt-assisted deformation are observed in lower crust and mantle rocks exposed at oceanic core complexes from slow-spreading MORs[48], where the sporadic addition of melts or fluids has been invoked as a necessary trigger mechanism of deep detachment faulting[49]. Last, mafic veins and deformation fabrics seem to control the distribution of serpentine and carbonate-rich veins, formed by interaction with seawater during the later stages of exhumation of the sequence to the seafloor (Fig. 6c, d).

Formation of a scattered magmatic crust in an embryonic ocean

A key finding of Expedition 402 is the absence of recovered igneous crust, while the previous ODP Leg 107 recovered two ~100 m long basaltic sections in the vicinity of the Gortani ridge (Site 655) and the central Vavilov basin (Site 651)[24] (Fig. 1b). The Tyrrhenian oceanic plutonic material drilled so far is restricted to limited mafic intrusions and veins (olivine gabbro to gabbro, norite, diorite, and diabase), making <10% of the entire recovered basement (Supplementary Fig. 4a, b). The MORB-type plutonic magmatism in the Tyrrhenian COT was thereby limited to a few sporadic mafic intrusions, often converted to rodingites, mainly documented at Site U1616. In line with the scarcity of igneous crust, our drilled section agrees with seismic data[20–23] and show that the MORB-like basalt flows sampled by ODP Leg 107[26] (Fig. 1b) do not continuously overlie the exhumed peridotites. Thus, despite magma was produced by mantle upwelling in the underlying asthenosphere, the nascent Tyrrhenian oceanic igneous crust was formed by sporadic intrusions in an exhuming, refertilized mantle. Indeed, some proportion of magma produced in the asthenosphere were retained within the mantle without the formation of a continuous plutonic crust[16]. The occurrence of melt-bearing zones could have promoted strain localization and the formation of lithospheric shear zones, leading to an efficient process of mantle exhumation[18]. While the infiltration of small aliquots of magma facilitates mantle exhumation, the development of deep-rooted detachment faults produces a cool thermal structure beneath the footwall, possibly decreasing melt production[50]. Mantle refertilization and prolonged lithospheric thinning through detachment faulting, hence, might have delayed the development of a steady-state spreading center.

Limited melt focusing is further indicated by another remarkable discovery of the IODP Expedition 402: the occurrence of phlogopite, plagioclase, amphibole-, and apatite-rich magmatic intrusions (2 wt% K_2O, 0.6 wt% TiO_2, 31.2 wt% MgO, 8.1 wt% Al_2O_3, and 14.7 wt% CaO; Supplementary Data 2) crosscutting the exhumed mantle section. At Site U1614, these intrusions occur either as irregular patches or as late-stage cm-scale veins cross-cutting the serpentinite fabric of the host peridotite (Figs. 3d; 6a, b and Supplementary Fig. 4c, d). The occurrence of hydrous potassic intrusions elevates the Al_2O_3 and K_2O content in the associated lherzolite and dunite samples, such as those located at depths 350 and 360 mbsf at Site U1614 (Fig. 2 and Supplementary Fig. 3). The widespread refertilization recorded by the lherzolites and the injections of these potassic melts are linked, but the crosscutting relationships suggest two different stages of melt percolation. Indeed, while hydrous potassic intrusions are rare and randomly widespread in the entire section, the high Al-Ti-K contents of the refertilized peridotites are a common feature of the plagioclase-bearing lherzolite, with no spatial relationships with the late-stage potassic magmatic veins (Fig. 2). The location of the drilled sections in a back-arc environment suggests a contribution from the subducted slab in the formation of these hydrous potassic melts. It is worth noting, however, that magmatic intrusions with the same mineralogical association are reported in the Iberia-Newfoundland COT[15], where initial decompression melting taps these fertile reservoirs before pervasive partial melting and mantle depletion beneath a mature spreading center[15]. Magmatism with an enriched geochemical signature seems thereby a characteristic of embryonic stages of oceanic

https://doi.org/10.1038/s41467-025-57121-0

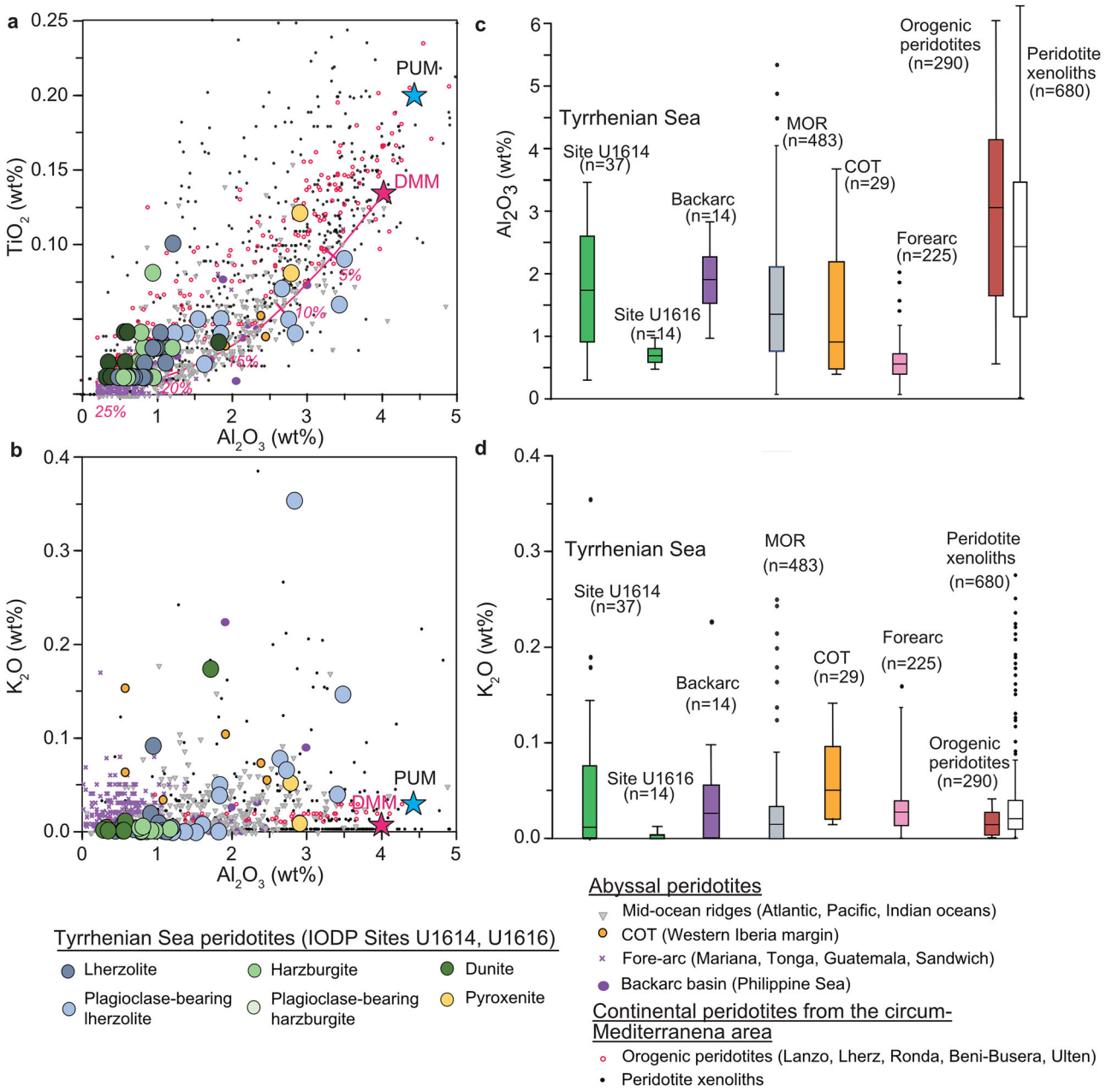

Fig. 5 | Whole-rock geochemistry of the IODP Sites U1614 and U1616 peridotites compared to peridotites from other geodynamic settings. Covariations in Al_2O_3 versus (**a**) TiO_2 and (**b**) K_2O contents and comparison between (**c**) Al_2O_3 and (**d**) K_2O contents between the Tyrrhenian Sea peridotites and abyssal peridotites from mid-ocean ridges (MOR)[57,58], back-arc basin[59], Continent-Ocean Transitions (COT) and fore-arc peridotites[54]. Compositions of orogenic peridotites and mantle xenoliths from the circum-Mediterranean area are compiled from the PetDB database (https://search.earthchem.org/). In (**a**), the compositions of abyssal peridotites are compared to the Al_2O_3 versus TiO_2 compositions of mantle residues of fractional melting. Residual mantle compositions were thermodynamically calculated using pMELTS[60] included in alphaMELTS software package[61]. Depleted-MORB Mantle (DMM) composition[62] (K, P, and Cr were excluded) was chosen as source material. Isentropic near fractional melting of DMM was conducted at pressures ranging from 3 to 1×10^{-4} GPa at 1450 °C. The melting trend is depicted in pink, and values of melting degrees are in pink italic numbers (see values in Supplementary Data 4).

evolution. In the Tyrrhenian Sea, these melts impart a potassic flavor to the mantle and may be involved in the origin of widespread MgO-rich potassic-ultrapotassic magmatism in the Italian peninsula[51].

In conclusion, we show here that the penultimate IODP Expedition on the R/V JOIDES Resolution has recovered some exceptional mantle lithologies from the Tyrrhenian embryonic COT. Contrary to the conventional view that the amagmatic or magma-poor nature of rifts is due to prolonged mantle upwelling of the melt-depleted refractory mantle, drilling deep into the Tyrrhenian embryonic oceanic mantle disclosed its real nature: a heterogeneous mantle produced by injections of heterogeneous magmas. These findings may prove that the inception of oceanic crust in this magma-poor margin was deferred by the exhumation of a hybridized mantle lithosphere. Hence, the two drillholes into the embryonic Tyrrhenian Sea will provide the opportunity to re-evaluate models of the birth of a new ocean before widespread asthenospheric upwelling allows volumetrically significant melt production leading to steady-state seafloor spreading. This study shows that our enhanced understanding of several fundamental geological processes has been achieved following oceanographic expeditions, particularly, those aimed at drilling the Earth's mantle.

https://doi.org/10.1038/s41467-025-57121-0

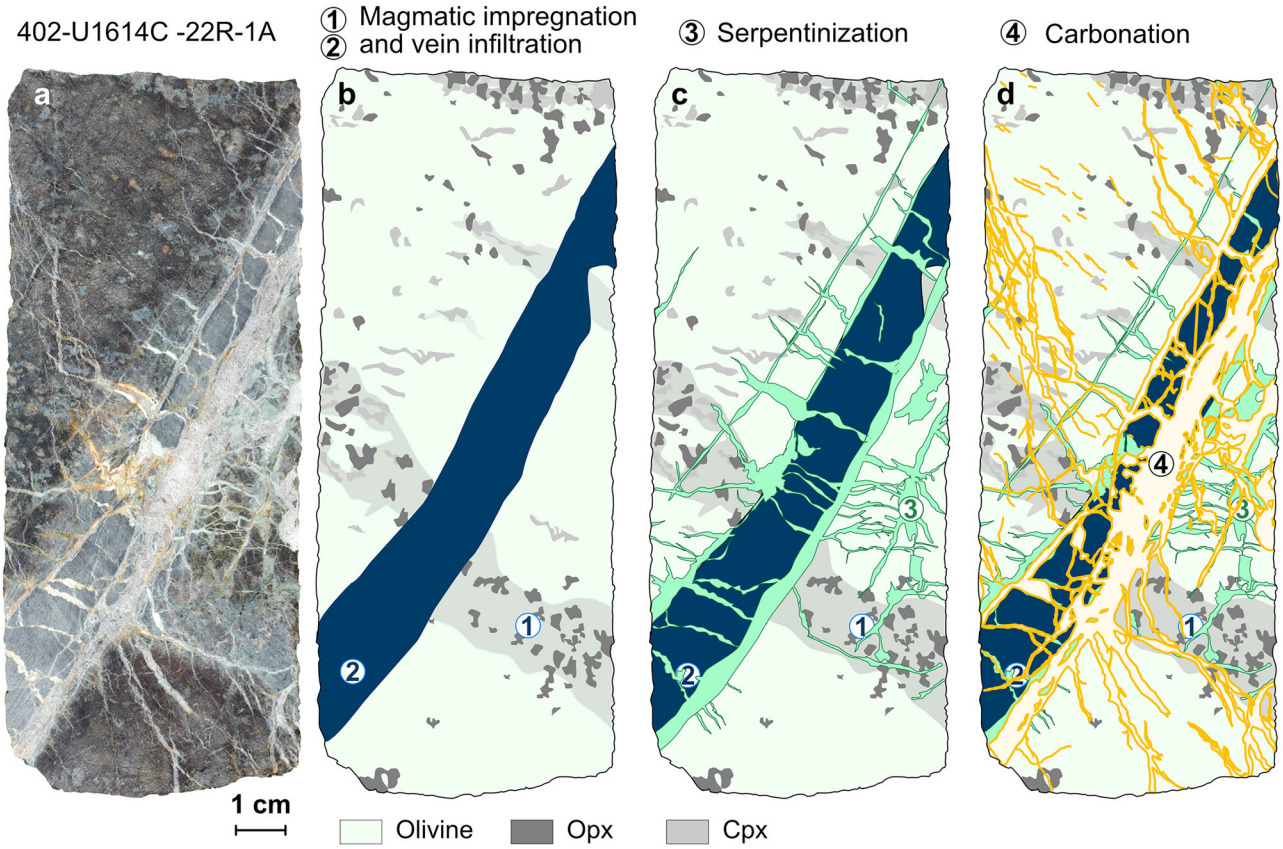

Fig. 6 | Core observations and associated sketches showing the evolution of the microstructure and mineral composition from high to low temperature conditions. a Photograph of core U1614C-22R-1A (interval 135/150 cm). **b** Mantle fabric is usually at a high angle to the core reference frame (> 40°) and here consists in a weak deformation subparallel to pyroxene-rich veins (1). A mafic intrusion (2, in blue) cuts this mantle fabric at a high angle. **c** Two generations of centimeter-scale serpentine veins (3, in pale green) follow pre-existing lithological contrasts or cut the magmatic vein-peridotite contacts. **d** Carbonate veins dissect the pre-existing features, overprinting both the initial mantle fabric and the serpentine vein network (4, in yellow).

Methods

All the data shown in this article have been produced onboard JOIDES Resolution during IODP Expedition 402. Bulk-rock geochemical analyses were obtained following the standard analytical protocols of ODP[52], also followed in previous IODP Expeditions (e.g., ref. 53), and will be hereafter briefly described. Geochemical data are reported in Supplementary Data 1 and 2.

Bulk-rock geochemistry

Major, minor, and trace elements were obtained using an Agilent 5110 inductively coupled plasma-atomic emission spectrometry (ICP-AES). Rock samples consisted of ~ 2 to 8 cm^3 of material cut from the core with a diamond saw blade. Saw marks, alteration rinds, and a by-product of the drilling process, were carefully removed from the outer surfaces of the rock samples by grinding on a diamond-impregnated grinding wheel. Each sample was then sonicated for 15 min in acetone. After decanting of the acetone, the samples were then sonicated twice more in nanopure deionized water for 10 min. The cleaned samples were dried for 10–12 h at 110 °C and afterward were crushed to < 1 cm chips using two disks of Delrin plastic installed in a Jaw Crusher hydraulic press. A SPEX 8515 Shatterbox powdering system with a tungsten carbide mill was then used to grind the chips to a fine powder for 3 min. Then, a ~ 5 g aliquot of the sample powder was weighed on a Mettler Toledo balance and ignited at 950 °C using a quartz crucible for 4 h to determine loss on ignition (LOI) with an estimated precision of 0.02 g (0.4%).

Ignited powders of 100.0 ± 0.2 mg were weighed and mixed with 400.0 ± 0.5 mg of lithium metaborate ($LiBO_2$) flux. Samples and standards were weighed on a Cahn C-31 microbalance designed to measure on a moving platform, with weighing errors of ± 0.05 mg under relatively smooth sea conditions. Standard rock powders and full procedural blanks were included with unknowns in each ICP-AES run. To prevent cooled glass beads from sticking to a crucible, a 10 µL aliquot of 0.172 mM aqueous LiBr solution was added to the mixture of flux and rock powder as a nonwetting agent. Samples were fused individually in Pt-Au (95:5) crucibles for 12 min at a maximum temperature of 1050 °C in an internally rotating induction furnace (Bead Sampler NT-4100). After cooling, beads were transferred to 125 mL high-density polypropylene (HDPE) bottles and dissolved in 50 mL of 10% (by volume) dilution of concentrated trace-metal grade HNO_3 (10% HNO_3, hereafter), aided by shaking with a Burrell wrist-action bottle shaker for 2 h. After digestion of the glass beads, the solutions were passed through a 0.45 µm filter into a clean 60 mL wide-mouth HDPE bottle. The solutions for major, minor, and trace element analyses were prepared from the filtered solutions, with a final solution-to-sample dilution factor of 5000 ×. The final solutions were prepared by pipetting 0.5 mL into a polyethylene centrifuge tube, which was diluted with 4.4 mL of 10 wt% HNO_3 and 0.1 mL of an internal standard solution containing Be, In, and Sb (final concentration of 100 µg/L Be and In and 200 µg/L Sb).

Major (Al, Ca, Fe, K, Mg, Mn, Na, Si, and Ti) and trace (Ba, Co, Cr, Cu, Ni, P, Sc, Sr, V, Y, Zn, and Zr) element concentrations of standards and samples were determined using an Agilent 5110 ICP-AES. Plasma

was ignited for at least 30 min before each run of samples to allow the instrument stabilization and warm-up time. Each sample was analyzed three times from the same dilute solution within a given sample run. Typically, 12 unknown samples were analyzed during a single run. A 10% HNO_3 rinse solution was run for 90 s between each sample analysis. Procedural blank solutions were run at the beginning and end of each run. Certified international rock reference materials run as calibration, drift, and quality check standard solutions were included with the unknown samples for each sample run. Certified international rock reference materials for calibration standard solutions were peridotites JP-1 and DTS-1, basalts BIR-1, BCR-2, JB-1b, and JB-2a, gabbros MRG-1 and JGb-1, andesite AGV-1, granite JG-2 and carbonate NBS-1C. Two certified international rock reference materials of basalt BHVO-2 and peridotite JP-1 were chosen for their compositional similarity to that of the analyzed material and were run as unknowns to check the precision and accuracy of major and trace analyses.

After drift correction using internal standards (Be, In, Sb) and subtraction of the procedural blank, a calibration line for each element was calculated using the results for the certified rock standards by Agilent's ICP Expert software. Concentrations used for the calibrations were compiled from literature[52]. Total Fe oxide concentrations were reported as $Fe_2O_3^T$ (Supplementary Data 1). Estimates of accuracy and precision of major and trace element analyses were based on the standard deviation between the three analyses of each sample and the replicate analyses of check standards, compared to published values. During the expedition, run-to-run relative standard deviation (RSD) by ICP-AES was generally ± 1–5% for major elements and ± 1–15% for trace elements. The RSD of P_2O_5 in peridotite JP-1 was exceptionally high, up to 21%, because P_2O_5 content is extremely low down to 0.005 wt% in JP-1 (Supplementary Data 3).

Total inorganic carbon

Total inorganic carbon (TIC) content was measured by quantifying the carbon dioxide (CO_2) released from an acidification process on carbonate minerals using a UIC Coulometrics 5017 CO_2 coulometer. Approximately 10– 12 mg of dried rock powders prepared for ICP-AES analyses were accurately weighed into a clean glass vial using two electronic balances and a computer averaging system that corrects for ship motion (Cahn C-31 automated electrobalance). Then, the rock powders were reacted with 5.0 mL of 1 M HCl on a hot plate set at 50°C, resulting in a release of CO_2. This reaction converts any present carbonate to CO_2. The liberated CO_2 was then transferred with an N_2 carrier gas to a coulometer cell filled with a solution containing excess monoethanolamine and a colorimetric pH indicator. As the gas passed through the coulometer cell, CO_2 was quantitatively absorbed and reacted with the monoethanolamine to form the carbamate salt of monoethanolamine. This solution was titrated with electrochemically generated OH^- to a colorimetric endpoint, and the corresponding change in light transmittance in the coulometric cell was monitored with a photodetection cell. This change in light transmittance was proportional to the TIC content of the sample. If a sample only contains calcium carbonates, all the evolved CO_2 was derived from the dissolution of calcium carbonate, and the TIC content was measured 5 min after the beginning of the reaction. The weight percent of calcium carbonate was calculated from the inorganic carbon content using the following equation:

$$CaCO_3(wt\%) = TIC(wt\%) \times 100/12 \quad (1)$$

A weighed amount of standard calcium carbonate (> 99.9%, $CaCO_3$, Fisher Scientific) and standard dolomite ($MgCa(CO_3)_2$, British Chemical Standards no. 368) was used to monitor analytical precision (1.46%) and accuracy (less than 1%). The measured data is presented in Supplementary Data 2.

Data availability

The measured geochemical data on the rocks and standards reported in this study are presented in Supplementary Data 1, 2 and 3. Results of alphaMELTS modeling is presented in Suppementary Data 4. The data are available in Figshare: https://doi.org/10.6084/m9.figshare.27153891. Additional structural and lithological data are available in the Preliminary Report of IODP Expedition 402 at: http://publications.iodp.org/preliminary_report/402/. More extensive data sets are available in the Expedition 402 Proceedings volume at: http://publications.iodp.org/proceedings/402/402/title.html an https://doi.org/10.14379/iodp.proc.402.2025

References

1. Cannat, M. et al. Proceedings of the ocean drilling program. *Init. Rep.* **153**, 5–13 (1995).
2. Kelemen, P. B. et al. *Leg 209 Summary*. **209** (2004).
3. McCaig, A. et al. Expedition 399 preliminary report: Building blocks of life, atlantis massif. International Ocean Discovery Program. https://doi.org/10.14379/iodp.pr.399.2024 (2024).
4. Gillis, K. et al. Proceedings of the Ocean drilling program. *Init. Rep.* **147**, 109–159 (1993).
5. Lissenberg et al. A long section of serpentinized depleted mantle peridotite. *Science* **385**, 623–629 (2024).
6. Boillot, G. et al. Proceedings of the Ocean drilling program. *Sci. Res.* **103**, 505–512 (1988).
7. Whitmarsh, R. B. et al. Site 1068. *Proc. Ocean Drill. Prog. Init. Rep.* **173**, 163–218 (1998).
8. Whitmarsh, R. B., Manatschal, G. & Minshull, T. A. Evolution of magma-poor continental margins from rifting to seafloor spreading. *Nature* **413**, 150–154 (2001).
9. Mohn, G. et al. Mode of continental breakup of marginal seas. *Geology* **50**, 1208–1213 (2022).
10. Pérez-Gussinyé, M. et al. Towards a process-based understanding of rifted continental margins. *Nat. Rev. Earth Env.* **4**, 166–184 (2023).
11. Pérez-Gussinyé, M. & Reston, T. J. Rheological evolution during extension at nonvolcanic rifted margins: Onset of serpentinization and development of detachments leading to continental breakup. *J. Geophys. Res.* **106**, 3961–3975 (2001).
12. Lavier, L. L. & Manatschal, G. A mechanism to thin the continental lithosphere at magma-poor margins. *Nature* **440**, 324–328 (2006).
13. Müntener, O. & Manatschal, G. High degrees of melt extraction recorded by spinel harzburgite of the Newfoundland margin: The role of inheritance and consequences for the evolution of the southern North Atlantic. *Earth Planet. Sci. Lett.* **252**, 437–452 (2006).
14. Péron-Pinvidic, G. & Manatschal, G. The final rifting evolution at deep magma-poor passive margins from Iberia-Newfoundland: a new point of view. *Int. J. Earth Sci.* **98**, 1581–1597 (2009).
15. Jagoutz, O. et al. The rift-to-drift transition in the North Atlantic: A stuttering start of the MORB machine? *Geology* **35**, 1087–1090 (2017).
16. Gillard, M. et al. Birth of an oceanic spreading center at a magma-poor rift system. *Sci. Rep.* **7**, 15072 (2017).
17. Pérez-Gussinyé, M., Morgan, J. P., Reston, T. J. & Ranero, C. R. The rift to drift transition at non-volcanic margins: Insights from numerical modelling. *Earth Planet. Sci. Lett.* **244**, 458–437 (2006).
18. Larsen, H. C. et al. Rapid transition from continental breakup to igneous oceanic crust in the South China Sea. *Nat. Geosci.* **11**, 782–789 (2018).
19. Sapin, F., Ringenbach, J.-C. & Clerc, C. Rifted margins classification and forcing parameters. *Sci. Rep.* **11**, 8199 (2021).
20. Malinverno, A. & Ryan, W. B. F. Extension in the Tyrrhenian Sea and shortening in the Apennines as result of arc migration driven by sinking of the lithosphere. *Tectonics* **5**, 227–245 (1986).

21. Faccenna, C., Funiciello, F., Giardini, D. & Lucente, P. Episodic back-arc extension during restricted mantle convection in the Central Mediterranean. *Earth Planet. Sci. Lett.* **187**, 105–116 (2001).
22. Prada, M., Ranero, C. R., Sallarès, V., Zitellini, N. & Grevemeyer, I. Mantle exhumation and sequence of magmatic events in the Magnaghi–Vavilov Basin (Central Tyrrhenian, Italy): New constraints from geological and geophysical observations. *Tectonophys* **689**, 133–142 (2016).
23. Loreto, M. F., Zitellini, N., Ranero, C. R., Palmiotto, C. & Prada, M. Extensional tectonics during the Tyrrhenian back-arc basin formation and a new morpho-tectonic map. *Basin Res.* **33**, 138–158 (2021).
24. Beccaluva, L et al. in *Proceedings Ocean Drilling Program, Scientific Results*. 107, (1990).
25. Kastens, K. & Mascle, J. The geological evolution of the Tyrrhenian Sea: An introduction to the scientific results of ODP Leg 107. *Proc. Ocean Drill. Prog. Sci. Res.* **107**, 3–26 (1990).
26. Bonatti, E., Seyler, M., Channell, J., Giraudeau, J. & Mascle, G. Peridotites drilled from the Tyrrhenian Sea, ODP Leg 107. *Proc. Ocean Drill. Prog. Sci. Res.* **107**, 37–47 (1990).
27. Kelemen, P. B. Reaction between ultramafic rock and fractionating basaltic magma I. Phase relations, the origin of calc-alkaline magma series, and the formation of discordant dunite. *J. Petrol.* **31**, 51–98 (1990).
28. Suhr, G. Melt migration under oceanic ridges: Inferences from reactive transport modelling of upper mantle hosted dunites. *J. Petrol.* **40**, 575–599 (1999).
29. Dygert, N. & Liang, Y. Temperatures and cooling rates recorded in REE in coexisting pyroxenes in ophiolitic and abyssal peridotites. *Earth Planet. Sci. Lett.* **420**, 151–161 (2015).
30. Sanfilippo, A., Salters, V., Tribuzio, R. & Zanetti, A. Role of ancient, ultra-depleted mantle in Mid-Ocean-Ridge magmatism. *Earth Planet. Sci. Lett.* **511**, 89–98 (2019).
31. Ongunyele, A. C. et al. Transition from orogenic-like to anorogenic magmatism in the Southern Alps during the Early Mesozoic: Evidence from elemental and Nd-Sr-Hf-Pb isotope geochemistry of alkali-rich dykes from the Finero Phlogopite Peridotite, Ivrea–Verbano Zone. *Gondwana Res.* **129**, 201–219 (2024).
32. González-Jiménez, J. M. et al. The architecture of the European-Mediterranean lithosphere: A synthesis of the Re-Os evidence. *Geology* **41**, 547–550 (2013).
33. Nicolas, A., Bouchez, J. L. & Mercier, J. C. Textures, structures and fabrics due to solid state flow in some European lherzolites. *Tectonophysics* **12**, 55–86 (1971).
34. Dick, H. J. B. & Bullen, T. Chromian spinel as a petrogenetic indicator in abyssal and alpine-type peridotites and spatially associated lavas. *Contrib. Mineral. Petrol.* **86**, 54–76 (1984).
35. Loocke, M., Snow, J. E. & Ohara, Y. Melt stagnation in peridotites from the Godzilla megamullion oceanic core complex, Parece Vela basin Philippine Sea. *Lithos* **182–183**, 1–10 (2013).
36. Sani, C., Sanfilippo, A., Peyve, A. A., Genske, F. & Stracke, A. Earth mantle's isotopic record of progressive chemical depletion. *AGU Adv.* **4**, https://doi.org/10.1029/2022AV000792 (2023).
37. Warren, J. M. Global variations in abyssal peridotite compositions. *Lithos* **248–251**, 193–219 (2016).
38. Borghini, G. et al. Fast REE re-distribution in mantle clinopyroxene via reactive melt infiltration. *Geochem. Perspect. Lett.* **26**, https://doi.org/10.7185/geochemlet.2323 (2023).
39. Warren, J. M. & Shimizu, N. Cryptic variations in abyssal peridotite compositions: Evidence for shallow-level melt infiltration in the oceanic lithosphere. *J. Petrol.* **51**, 395–423 (2010).
40. Trua, T., Clocchiatti, C., Schiano, P., Ottolini, L. & Marani, M. The heterogeneous nature of the Southern Tyrrhenian mantle: Evidence from olivine-hosted melt inclusions from back-arc magmas of the Marsili seamount. *Lithos* **118**, 1–16 (2010).
41. Zitellini, N., Malinverno, A. & Estes, E. R. International Ocean discovery program. Expedition 402 scientific prospectus: Tyrrhenian continent–Ocean transition. https://doi.org/10.14379/iodp.sp.402.2023 (2023).
42. Bodinier, J.-L., Garrido, C. J., Chanefo, I., Bruguier, O. & Gervilla, F. Origin of pyroxenite–peridotite veined mantle by refertilization reactions: Evidence from the Ronda peridotite (southern Spain). *J. Petrol.* **49**, 999–1025 (2008).
43. Rampone, E., Piccardo, G. B., Vannucci, R., Bottazzi, P. & Ottolini, L. Subsolidus reactions monitored by trace element partitioning: the spinel- to plagioclase-facies transition in mantle peridotites. *Contrib. Mineral. Petrol.* **115**, 1–17 (1993).
44. Garrido, C. J. & Bodinier, J. L. Diversity of mafic rocks in the Ronda peridotite: Evidence for pervasive melt–rock reaction during heating of subcontinental lithosphere by upwelling asthenosphere. *J. Petrol.* **40**, 729–754 (1999).
45. Morishita, T., Arai, S., Gervilla, F. & Green, D. H. Closed-system geochemical recycling of crustal materials in alpine-type peridotite. *Geochim. Cosmochim. Acta* **67**, 303–310 (2003).
46. Ferrando, C. et al. Deep segregation and crystallization of ultra-depleted melts in the sub-ridge mantle. *Chem. Geol.* **644**, 121840 (2024).
47. Ceuleneer, G. & Cannat, M. High-temperature ductile deformation of site 920 peridotites. *Proc. Ocean Drill. Prog. Sci. Res.* **153**, 23–34 (1997).
48. Dick, H. J. B. et al. Dynamic accretion beneath a slow-spreading ridge segment: IODP Hole 1473A and the Atlantis Bank oceanic core complex. *J. Geophys. Res.* **124**, 12631–12659 (2019).
49. Bickert, M., Lavier, L. & Cannat, M. How do detachment faults form at ultraslow mid-ocean ridges in a thick axial lithosphere? *Earth Planet. Sci. Lett.* **533**, 116048 (2020).
50. Mezri, L. et al. Tectonic controls on melt production and crustal architecture during magma-poor seafloor spreading. *Earth Planet. Sci. Lett.* **628**, 118569 (2024).
51. Conticelli, S. et al. Trace elements and Sr–Nd–Pb isotopes of K-rich, shoshonitic, and calc-alkaline magmatism of the Western Mediterranean Region: Genesis of ultrapotassic to calc-alkaline magmatic associations in a post-collisional geodynamic setting. *Lithos* **107**, 68–92 (2009).
52. Murray, R., Miller, D. J., Kryc, K. Analysis of major and trace elements in rocks, sediments, and interstitial waters by inductively coupled plasma–atomic emission spectrometry (ICP-AES). ODP Technical Note 29 https://doi.org/10.2973/odp.tn.29.2000 (2000).
53. Planke, S., Berndt, C., Alvarez Zarikian, C. A., and the Expedition 396 Scientists. Mid-Norwegian margin magmatism and Paleoclimate implications. In *Proceedings of the International Ocean Discovery Program*, 396: College Station, TX (International Ocean Discovery Program, 2023).
54. Parkinson, I. J. & Pearce, J. A. Peridotites from the Izu–Bonin–Mariana forearc (ODP Leg 125): Evidence for mantle melting and melt–mantle interaction in a supra-subduction zone setting. *J. Petrol.* **39**, 1577–1618 (1988).
55. Ohara, Y. et al. Peridotites from the Mariana Trough: first look at the mantle beneath an active back-arc basin. *Contrib. Mineral. Petrol.* **143**, 1–18 (2002).
56. Ohara, Y., Fujioka, K., Ishii, T. & Yurimoto, H. Peridotites and gabbros from the Parece Vela backarc basin: Unique tectonic window in an extinct backarc spreading ridge. *Geochem. Geophys. Geosys.* **4**, 8611 (2003).
57. Debret, B., Andreani, M. & Godard, M. A review of abyssal serpentinite geochemistry and geodynamics. *Earth Sci. Rev.* **258**, 104910 (2024).
58. Niu, Y. Bulk-rock major and trace element compositions of abyssal peridotites: Implications for mantle melting, melt extraction and post-melting processes beneath mid-ocean ridges. *J. Petrol.* **45**, 2423–2458 (2004).

59. Akizawa, N. et al. Geochemical characteristics of back-arc basin lower crust and upper mantle at final spreading stage of Shikoku Basin: an example of Mado Megamullion. *Prog. Earth Planet. Sci.* **8**, 65 (2021).
60. Ghiorso, M. S., Hirschmann, M. M., Reiners, P. W. & Kress, V. C. The pMELTS: A revision of MELTS for improved calculation of phase relations and major element partitioning related to partial melting of the mantle to 3 Gpa. *Geochem. Geophys. Geosys.* **3**, 1–35 (2002).
61. Smith, P. M. & Asimow, P. D. Adiabat_1ph: A new public front-end to the MELTS, pMELTS, and pHMELTS models. *Geochem. Geophys. Geosys*. https://doi.org/10.1029/2004GC000816 (2005).
62. Workman, R. K. & Hart, S. R. Major and trace element composition of the depleted MORB mantle (DMM). *Earth Planet. Sci. Lett.* **231**, 53–72 (2005).

Acknowledgements

This research used samples and data generated during the International Ocean Discovery Program (IODP) Expedition 402 on the JOIDES Resolution. We are grateful to the JOIDES Resolution Science Operator staff as well as the Siem Offshore crew members who made the expedition possible. E.R.E. was supported through NSF award OCE–1326927. L.M.'s PhD scholarship is supported by Geoscience Australia. W.M. is supported by the H2020 MSCA-IF – TURBOMUD project – GA No. 101018321. Support for E. Estes was provided by NSF grants OCE1326927 (IODP JRSO) and OCE2412279 (IODP Closeout). Gianreto Manatschal, Darin Schwartz, and three anonymous reviewers are thanked for their comments and suggestions that improved the earlier versions of the manuscript.

Author contributions

N.Z., M.F.L., D.B., and C.G. conceived the project and contributed to the original IODP proposal. E.R.E., A.M., and N.Z. led Expedition 402. M.B., C.L., T.M., A.P., E.P., A.S., and P.V. performed the petrographic and structural description of mantle peridotites and associated lithologies. Nak, E.C., S.G., and Q.F. performed the whole-rock geochemical analysis. Nab, I.F., M.F.L., B.S., P.P., V.P., and X.Z. measured the physical and magnetic properties of the peridotites. L.K., L.M., and W.M. described the peridotite-sediments interface and sedimentary lithologies. A.D.S. and R.K.K. constructed the preliminary age model of the sediments. M.R.P. quantified biogeochemical cycling of elements. All authors contributed equally to the interpretation of the data. A.S. and A.P. wrote the text with contributions from all authors.

Competing interests

The authors declare no competing interests.

Additional information

Supplementary information The online version contains supplementary material available at https://doi.org/10.1038/s41467-025-57121-0.

Correspondence and requests for materials should be addressed to Alessio Sanfilippo.

Peer review information *Nature Communications* thanks Gianreto Manatschal and Darin Schwartz for their contribution to the peer review of this work. A peer review file is available.

Reprints and permissions information is available at http://www.nature.com/reprints

Publisher's note Springer Nature remains neutral with regard to jurisdictional claims in published maps and institutional affiliations.

[1]Department of Earth and Environmental Science, University of Pavia, Pavia, Italy. [2]School of Earth, Environmental and Sustainability Sciences, Indian Institute of Science Education and Research Thiruvananthapuram, Kerala, India. [3]Atmosphere and Ocean Research Institute, University of Tokyo, Tokyo, Japan. [4]Department of Geology and Geophysics, Louisiana State University, Baton Rouge, LA, USA. [5]Department of Geology and Geophysics, University of Utah, Salt Lake City, USA. [6]Geo-Ocean, Univ Brest, CNRS, IFREMER, Plouzané, France. [7]College of Marine Science and Engineering, China University of Geosciences, Wuhan, China. [8]Earth Sciences Department, University of Florence, Florence, Italy. [9]International Ocean Discovery Program, Texas A&M University, College Station, Texas, USA. [10]Lamont-Doherty Earth Observatory, Columbia University, Palisades, USA. [11]Tono Geoscience Center, Japan Atomic Energy Agency (JAEA), Tokyo, Japan. [12]Department of Biological, Geological and Environmental Science, Earth Science Division, University of Catania, Catania, Italy. [13]Earth and Atmospheric Sciences, University of Nebraska, Lincoln, USA. [14]Department of Earth and Atmospheric Sciences, University of Houston, Houston, USA. [15]Laboratoire d'Océanographie et du Climat: Expérimentations et Approches Numériques, Sorbonne Université, Campus Pierre et Marie Curie, Paris, France. [16]University of Texas Institute for Geophysics, University of Texas at Austin, Austin, TX, USA. [17]Department of Earth Sciences, Binghamton University, New York, USA. [18]Institute of Marine Sciences - ISMAR, Italian National Research Council, Bologna, Italy. [19]Institute for Marine and Antarctic Studies (IMAS), University of Tasmania, Hobart, Australia. [20]Department of Marine Geosciences, ICM-CSIC, Barcelona, Spain. [21]Geosciences Montpellier, Montpellier, France. [22]Marine Biology, Texas A&M University at Galveston, Galveston, USA. [23]School of Oceanography, Shanghai Jiao Tong University, Shanghai, China. [24]Instituto Andaluz de Ciencias de la Tierra (IACT), Armilla Granada, Spain. [25]Dipartimento di Scienze Chimiche e Geologiche, Università di Modena e Reggio Emilia, Modena, Italy. [26]School of Geosciences and Civil Engineering, College of Science and Engineering, Kanazawa University, Kanazawa, Japan.
✉e-mail: alessio.sanfilippo@unipv.it